Article

Stability Analysis of Quantum-Dot Spin-VCSELs

Nianqiang Li [1], Dimitris Alexandropoulos [2], Hadi Susanto [3], Ian Henning [1] and Michael Adams [1,*]

[1] School of Computer Science and Electronic Engineering, University of Essex, Wivenhoe Park, Colchester CO4 3SQ, UK; nlic@essex.ac.uk (N.L.); idhenn@essex.ac.uk (I.H.)

[2] Department of Materials Science, University of Patras, Patras 26504, Greece; dalexa@upatras.gr

[3] Department of Mathematical Sciences, University of Essex, Wivenhoe Park, Colchester CO4 3SQ, UK; hsusanto@essex.ac.uk

[*] Correspondence: adamm@essex.ac.uk; Tel.: +44-120-687-2431

Abstract: Spin-polarized vertical-cavity surface-emitting lasers (spin-VCSELs) and vertical external-cavity surface-emitting lasers (spin-VECSELs) are of interest since their output polarization can be manipulated by spin-selective pumping, either optical or electrical. These devices, using quantum dot (QD) material for the active region, have shown instability (periodic oscillations) and polarization switching in previous theoretical simulations based on a rate equation model. It has been recognized that the polarization switching occurs between two possible sets of solutions, termed here in-phase and out-of-phase. The present contribution seeks to give enhanced understanding of these behaviors by applying a stability analysis to the system of equations used for such simulations. The results indicate that the choice of in-phase and out-of-phase solutions that appear in a time-dependent simulation is determined by the condition that the corresponding steady-state solutions are stable against small perturbations. The stability analysis is shown to be a valuable theoretical tool for future study of spin-V(E)SELs in the context of understanding and guiding future experimental research.

Keywords: laser; vertical cavity; polarization; spin; quantum dot; stability; instability; periodicity

1. Introduction

Vertical-cavity surface-emitting lasers (VCSELs), whose output polarization can be controlled by the creation of spin-polarized carrier concentrations, are an important class of spin-optoelectronic devices. The history of these devices, termed spin-VCSELs, can be traced back to 1997 when pulsed emission at twice the Larmor frequency and with alternating circular polarization was observed from a VCSEL in a magnetic field pumped with circularly polarized light at cryogenic temperature [1]. There followed the first reports of circularly polarized emission from a VCSEL pumped with circularly polarized light at room temperature [2] and of the output polarization ellipticity following the ellipticity of the optical pump [3]. Since then, there has been a steady increase of research interest in spin-VCSELs, fuelled in part by the prospects of lower thresholds than for conventional VCSELs [4] and of birefringence-related polarization oscillations at frequencies much higher than the usual limit imposed by the relaxation oscillation frequency [5]. A 2012 review paper [6] gives more background and an excellent introduction to the subject.

The principle of operation of a spin-VCSEL is based on the creation of a spin-polarized carrier population, either by electrical injection with a spin-polarized current [7] or by optical pumping with polarized light. For a quantum confined active material, the optical selection rules [6,7] dictate that spin-up (spin-down) electrons recombine radiatively with spin-up (spin-down) holes generating left (right) circularly-polarized photons. The need for a quantum confined active material means

that most spin-VCSEL research to date has been focused on quantum well (QW) materials, although advances in materials technology have led to an important line of research into quantum dot (QD) polarized light sources [8]. QD spin-VCSELs emitting at 983 nm have been successfully fabricated using a Schottky tunnel spin injection contact [9]; the maximum operating temperature reported is 230 K [10]. More recently, our group has reported the first QD spin-polarized vertical external-cavity surface-emitting laser (spin-VECSEL) [11]; this operates at room temperature and at the telecom wavelength of 1300 nm.

The present contribution deals with theoretical analysis of QD spin-V(E)CSELs. Rate equation models for these devices must describe the behaviour of two (complex) electric fields (right- and left-circularly polarized), two electron populations (spin-up and spin-down) in the ground state of the dots, and at least two other spin-polarized electron populations in the wetting layer, which acts as a reservoir for carriers. The spin-up and spin-down populations of holes in the dots and wetting layer can also be included [12,13], although in most cases it is adequate to assume that the spin relaxation of holes is instantaneous. Also, carrier populations in excited states of the dots can be included in a more general model [14,15]. Our group has developed a model [16,17] that, whilst only retaining equations for the minimum number of carrier populations, has included the addition of birefringence and dichroism in the equations for the electric fields to extend the well-known spin-flip model (SFM) [18] to deal with QD spin-lasers. This model has been applied to a study of instabilities [16] which occur under continuous wave (cw) pumping for certain conditions of pump polarization and intensity. In addition to regions of periodic oscillations at a frequency related to the birefringence rate (as previously predicted for QW spin-VCSELs [19]), conditions were also found where a form of polarization switching occurred, i.e., the sign of the output ellipticity could switch from being either the same as, or opposite to that of the pump [16]. Interestingly, our experimental studies of the 1300 nm QD spin-VECSEL [11] also revealed that different signs of output polarization ellipticity could be found at different positions on the wafer. However, it is too early to assume that the observed behaviour is caused by the same underlying physics as that of the model, since practical effects such as local thermally induced changes in birefringence might dominate in the experiment. Notwithstanding these practical results, the focus of the present work is to investigate the causes of the behaviour seen in our model and we do this by applying a stability analysis.

2. Model and Analysis

Our QD spin-VCSEL model has been described in detail in previous publications [16,17] and hence only a brief description is given here. Normalized variables are used for the conduction band carrier concentrations (*n*) with subscripts WL (wetting layer) and QD (quantum dot ground state), and superscripts + (spin-down) and − (spin-up). The normalized complex electric fields are denoted by $\overline{E}_+$ ($\overline{E}_-$) for right (left) circular polarization. Spin relaxation of carriers within the WL and the QD occurs at the same rate γ_j, and the carrier capture rate from WL to QD is denoted by γ_o. The polarized fields are coupled by the birefringence rate γ_p and also by the dichroism (gain anisotropy) γ_a. Recombination of carriers in the WL is neglected since it is assumed that capture into the ground state of the QD is the dominant process. Similarly, effects of excited states in the QD are not included, nor are escape of carriers from the QD back to the WL. Pauli blocking of carriers pumped into the WL is neglected, but the blocking effect of capture into the QD is included.

With these assumptions, the normalized complex rate equations for the system can be written as

$$\frac{d\overline{E}_{\pm}}{dt} = \kappa(n_{QD}^{\pm} - 1)(1 + i\alpha)\overline{E}_{\pm} - (\gamma_a + i\gamma_p)\overline{E}_{\mp} \tag{1}$$

$$\frac{dn_{WL}^{\pm}}{dt} = \eta_{\pm}\gamma_n + h\frac{\gamma_n}{2} - \gamma_o n_{WL}^{\pm}\left[\frac{h - n_{QD}^{\pm}}{2h}\right] \mp \gamma_j(n_{WL}^{+} - n_{WL}^{-}) \tag{2}$$

$$\frac{dn_{QD}^{\pm}}{dt} = \gamma_o\frac{n_{WL}^{\pm}}{h}(h - n_{QD}^{\pm}) - \gamma_n(h + n_{QD}^{\pm}) \mp \gamma_j(n_{QD}^{+} - n_{QD}^{-}) - 2\gamma_n n_{QD}^{\pm}\left|\overline{E}_{\pm}\right|^2 \tag{3}$$

where κ is the photon decay rate, α is the linewidth enhancement factor, η_+ (η_-) is the right (left) circularly polarized component of the pump and γ_n is the recombination rate of carriers from the QD ground state. The parameters γ_n, γ_j, γ_o, γ_p, γ_a, and κ have dimensions of inverse time and the parameter α is dimensionless. The dimensionless parameter h is a normalized gain coefficient defined by

$$h = v_g \Gamma a N_D \tau_p \tag{4}$$

where v_g is the group velocity, Γ is the optical confinement factor, a is the differential gain (or "interaction cross-section", dimension L^2), N_D is the density of dots per volume (sometimes written as the density per area divided by the layer thickness, dimension L^{-3}) and $\tau_p = (2\kappa)^{-1}$ is the photon lifetime.

Equations (1)–(3) constitute the set of coupled differential equations (eight real equations) to be solved for the time-dependence of the dimensionless variables representing field components and carrier concentrations for various values of the pump parameters (η_+, η_-). These last two are usually combined into the total normalized pump power $\eta = \eta_+ + \eta_-$ and the pump polarization ellipticity P defined as

$$P = \frac{\eta_+ - \eta_-}{\eta_+ + \eta_-} \tag{5}$$

Similarly, the spin-laser output is expressed in terms of circularly polarized intensities $I_+ = \left|\overline{E}_+\right|^2$, $I_- = \left|\overline{E}_-\right|^2$, $I_{total} = I_+ + I_-$, and polarization ellipticity ε defined as

$$\varepsilon = \frac{I_+ - I_-}{I_+ + I_-} \tag{6}$$

Values of P or ε of +1 (-1) correspond to right (left) circular polarization, whilst a value of 0 corresponds to linear polarization. Note that here we are assuming that in the case of QD active media where the degeneracy of heavy hole (hh) and light hole (lh) states is lifted, it is a reasonable approximation to ignore transitions between the conduction band and the lh states; hence, the polarization of the pump is correctly described by the terms (η_+, η_-) in the rate Equation (2) for WL electrons.

Our analysis of the stability of the solutions of Equations (1)–(3) follows the method presented earlier for the case of QW spin-VCSELs [20]. The time-independent solutions have the following form:

$$\overline{E}_+ = E_+ e^{i\omega t} \quad \overline{E}_- = E_- e^{i\theta} e^{i\omega t} \quad n_{WL}^\pm = n_{WL}^{s\pm} \quad n_{QD}^\pm = n_{QD}^{s\pm} \tag{7}$$

where the superscript 's' denotes the value in steady state. When the phase θ is the "continuation" of 0 or π, we refer to the solution as in-phase or out-of-phase, respectively. Carrying out a stability analysis, we write $\overline{E}_+ = \left(E_+ + \delta\hat{E}_+ e^{\lambda t}\right) e^{i\omega t}$, $\overline{E}_- = \left(E_- e^{i\theta} + \delta\hat{E}_- e^{\lambda t}\right) e^{i\omega t}$, $n_{WL}^\pm = n_{WL}^{s\pm} + \delta\hat{n}_{WL}^\pm e^{\lambda t}$, $n_{QD}^\pm = n_{QD}^{s\pm} + \delta\hat{n}_{QD}^\pm e^{\lambda t}$, and linearize for small δ to find the eigenvalue equation

$$M\underline{v} = \lambda\underline{v} \tag{8}$$

where $\underline{v} = \left(\hat{E}_+, \hat{E}_-, \hat{E}_+^*, \hat{E}_-^*, \hat{n}_{WL}^+, \hat{n}_{WL}^-, \hat{n}_{QD}^+, \hat{n}_{QD}^-\right)^T$, with the superscript 'T' denoting transpose and '*' denoting complex conjugation. The coefficient matrix reads:

$$M = \begin{bmatrix} M_{11} & M_{12} & 0 & 0 & 0 & 0 & K_1 E_+ & 0 \\ M_{12} & M_{22} & 0 & 0 & 0 & 0 & 0 & K_1 E_- e^{i\theta} \\ 0 & 0 & M_{11}^* & M_{12}^* & 0 & 0 & K_1^* E_+ & 0 \\ 0 & 0 & M_{12}^* & M_{22}^* & 0 & 0 & 0 & K_1^* E_- e^{-i\theta} \\ 0 & 0 & 0 & 0 & M_{55} & \gamma_j & M_{57} & 0 \\ 0 & 0 & 0 & 0 & \gamma_j & M_{66} & 0 & M_{68} \\ K_2 E_+ & 0 & K_2 E_+ & 0 & M_{75} & 0 & M_{77} & \gamma_j \\ 0 & K_3 E_- e^{-i\theta} & 0 & K_3 E_- e^{i\theta} & 0 & M_{86} & \gamma_j & M_{88} \end{bmatrix} \tag{9}$$

where

$$M_{11} = \kappa(n_{QD}^{s+} - 1)(1 + i\alpha) - i\omega \quad M_{12} = -(\gamma_a + i\gamma_p) \quad M_{22} = \kappa(n_{QD}^{s-} - 1)(1 + i\alpha) - i\omega$$

$$M_{55} = -\gamma_o \left[\frac{h - n_{QD}^{s+}}{2h} \right] - \gamma_j \quad M_{57} = \frac{\gamma_o n_{WL}^{s+}}{2h} \quad M_{66} = -\gamma_o \left[\frac{h - n_{QD}^{s-}}{2h} \right] - \gamma_j \quad M_{68} = \frac{\gamma_o n_{WL}^{s-}}{2h}$$

$$M_{75} = \frac{\gamma_o}{h}(h - n_{QD}^{s+}) \quad M_{77} = -\gamma_o \frac{n_{WL}^{s+}}{h} - \gamma_n - \gamma_j - 2\gamma_n E_+^2$$

$$M_{86} = \frac{\gamma_o}{h}(h - n_{QD}^{s-}) \quad M_{88} = -\gamma_o \frac{n_{WL}^{s-}}{h} - \gamma_n - \gamma_j - 2\gamma_n E_-^2$$

$$K_1 = \kappa(1 + i\alpha) \quad K_2 = -2\gamma_n n_{QD}^{s+} \quad K_3 = -2\gamma_n n_{QD}^{s-}$$

The solution is unstable when there is an eigenvalue with Re(λ) > 0 and stable when all the eigenvalues have Re(λ) < 0.

3. Results

We consider two sets of parameter values, as given in Table 1, corresponding to two hypothetical QD spin-VCSEL structures, denoted VCSEL1 and VCSEL2. These were chosen because simulation studies revealed that small changes in device parameters could result in different types of behavior. In this case, small changes in gain and alpha between VCSEL1 and VCSEL2 produced changes from oscillatory to polarization switching behavior, and as mentioned earlier, this has some similarities with variations seen in experimental observations [11]. VCSEL1 is the structure used for the results in Figures 3 and 4 of [16], whilst VCSEL2 has not been studied previously. It will be seen from the results to be presented below that the dynamic behavior of the QD spin-VCSEL is very sensitive to the choice of values for gain and linewidth factor, as is already well-known for other VCSELs (see, e.g., [19–21]).

Table 1. Values of parameters for two examples of quantum dot spin-vertical-cavity surface-emitting lasers (QD spin-VCSELs).

Parameter	Symbol	VCSEL1 Value	VCSEL2 Value
Photon decay rate	κ	250 ns^{-1}	250 ns^{-1}
Carrier recombination rate	γ_n	1 ns^{-1}	1 ns^{-1}
Capture rate into from WL into QD	γ_o	400 ns^{-1}	400 ns^{-1}
Spin relaxation rate	γ_j	10 ns^{-1}	10 ns^{-1}
Birefringence rate	γ_p	20 ns^{-1}	20 ns^{-1}
Dichroism rate	γ_a	0	0
Linewidth enhancement factor	α	3	4
Normalized gain coefficient	h	1.1995	1.05

3.1. Results for VCSEL1

Figure 1 shows calculated plots of the steady-state output polarization ellipticity versus the pump ellipticity for VCSEL1 at two values of normalized total pump intensity—(a) η = 1.2 and (b) η = 1.7. In each case, the in-phase (red) and out-of-phase (blue) curves are found from the steady-state solutions of Equations (1)–(3); the points marked as '*' are found by numerical integration of the time-dependent rate equations. It is clear that for each case of pumping there are regions where each of the in-phase and out-of-phase solutions are stable and a region where there is no stability [16]. Figure 2 shows corresponding results for the real parts of the critical eigenvalues versus the pump ellipticity, calculated from the solution of Equation (8), for the same values of pump intensity. The stability of the fixed points is lost through a Hopf bifurcation. It is clear that the regions of stability in the ellipticity results of Figure 1 correspond to those with negative real parts of the eigenvalues in Figure 2. Thus,

the stability analysis reveals that the sections of the in-phase and out-of-phase solutions that appear in a time-dependent solution are selected by the condition that the steady-state solutions are stable against small perturbations.
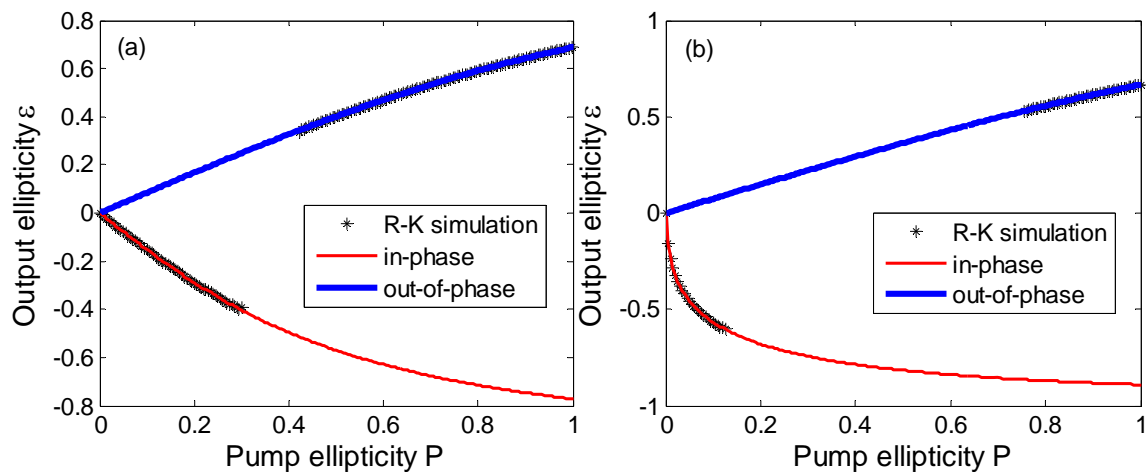

Figure 1. Output ellipticity vs. pump ellipticity for vertical-cavity surface-emitting laser 1 (VCSEL1) with (**a**) η = 1.2; and (**b**) η = 1.7.
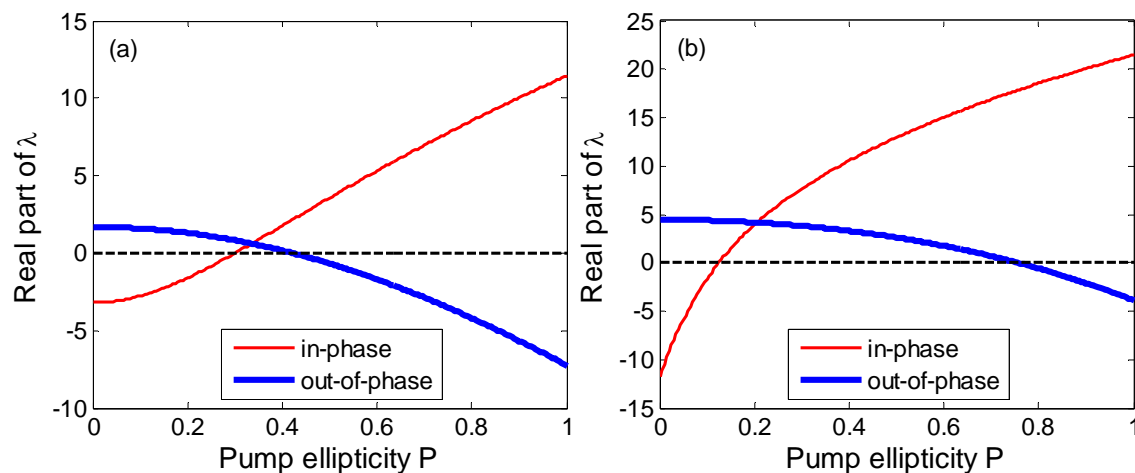

Figure 2. Real parts of the critical eigenvalues vs. pump ellipticity for VCSEL1 with (**a**) η = 1.2; and (**b**) η = 1.7.

Figure 3 shows examples of the simulated behavior in regions of instability for VCSEL1, again for the same values of pump intensity. Figure 3a shows periodic oscillations of the right- and left-circularly polarized components for η = 1.2, *P* = 0.35, and Figure 3b shows similar behavior for η = 1.7, *P* = 0.5. The frequency of oscillation for these examples is 6.9 GHz for the former and 7.7 GHz for the latter. For comparison, the frequency corresponding to the birefringence for VCSEL1 is given approximately [19] by $\gamma_p/\pi = 6.4$ GHz. By contrast, the relaxation oscillation frequency is given by [21] $[2\kappa\gamma_n(\eta - 1)]^{1/2}/(2\pi)$, which yields 1.6 GHz and 3.0 GHz for η = 1.2 and 1.7, respectively. Of course, for values η and *P* in regions of stability, we find continuous output with constant intensity in each polarized component.
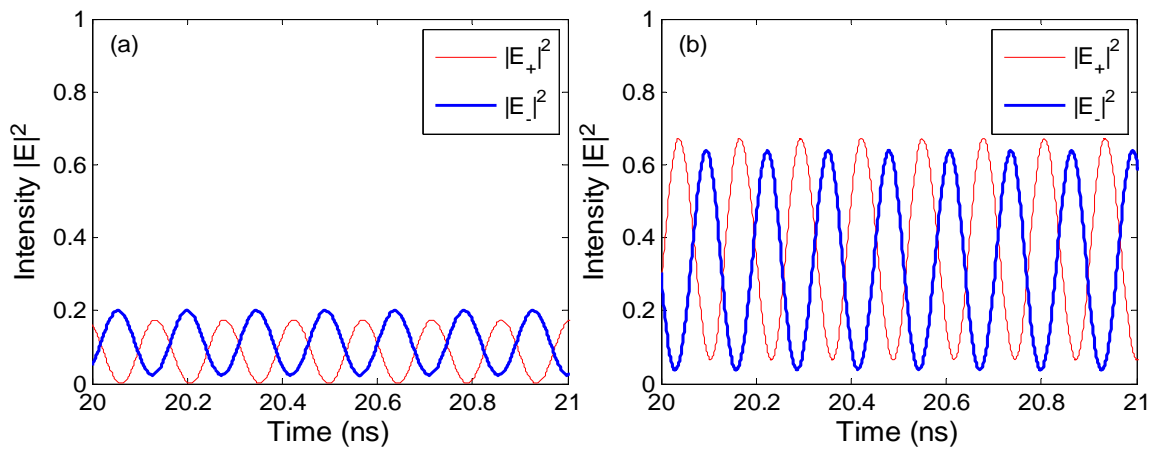
Figure 3. Circularly polarized intensity components vs. time for VCSEL1 with (**a**) η = 1.2, *P* = 0.35; and (**b**) η = 1.7, *P* = 0.5.

3.2. Results for VCSEL2

Figure 4, calculated from the time-dependent solution of the rate equations for VCSEL2, gives examples of a different type of behavior in the dependence of output ellipticity on pump ellipticity and intensity. The values of pump intensity here have been deliberately chosen to show specific forms of behavior. There is no region of instability; instead, the sign of the ellipticity switches abruptly in Figure 4a and exhibits bistability for the normalized pump intensity η = 1.1, whilst in Figure 4b there is no change of sign, so the output ellipticity always has the opposite sign to that of the pump for η = 1.9. This behavior is explained by the corresponding plots of the real parts of the eigenvalues versus |P| in Figure 5a. Here, for η = 1.1, there is always at least one real part that is negative over the whole range of |P|, whilst the real parts of both in-phase and out-of-phase eigenvalues are negative over the range 0.72 < |P| < 0.86. This accounts for the hysteresis of polarization over this region of |P| seen in Figure 4a. In Figure 5b, for η = 1.9, the real part of the in-phase eigenvalue is negative and that of the out-of-phase eigenvalue is positive over the entire range of |P|, thus successfully accounting for the behavior seen in Figure 4b.
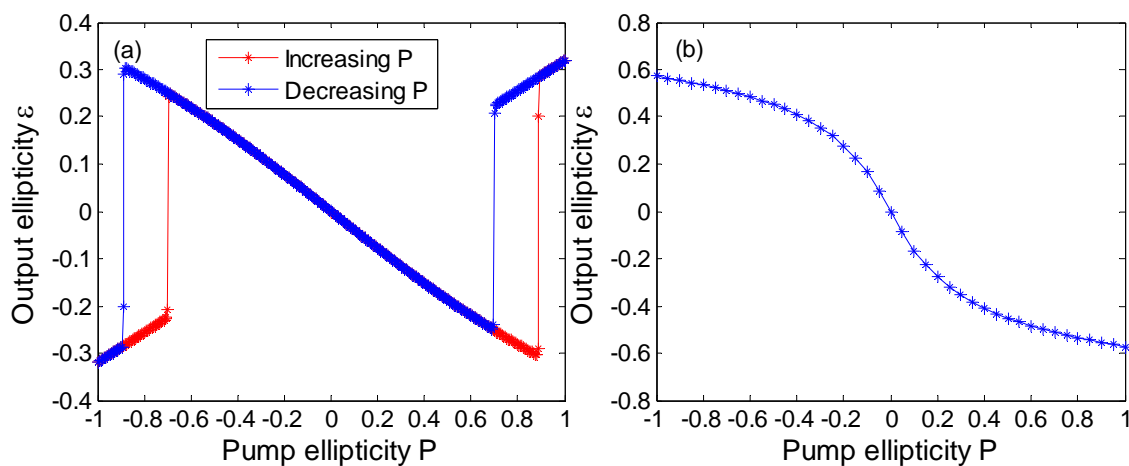

Figure 4. Output ellipticity vs. pump ellipticity for VCSEL2 with (**a**) η = 1.1; and (**b**) η = 1.9.
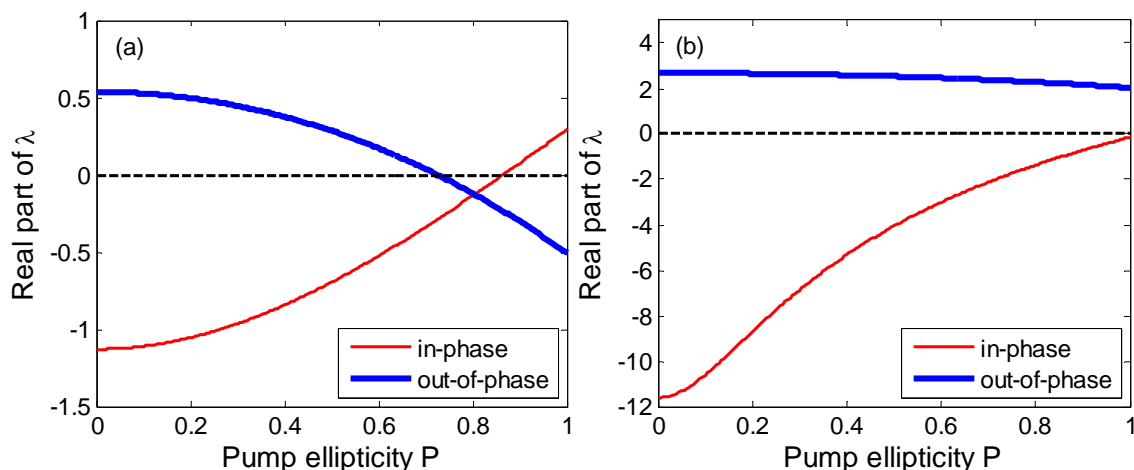
Figure 5. Real parts of eigenvalues vs. pump ellipticity for VCSEL2 with (**a**) $\eta = 1.1$; and (**b**) $\eta = 1.9$.

4. Conclusions

A stability analysis for QD spin-VCSELs has been presented which is an extended version of a similar analysis previously used for QW spin-VCSELs [16,17]. This has been applied to two hypothetical laser structures, one of which was previously simulated using a time-dependent solution of the rate equations. In the previous study [16], it was found that the sign of the output polarization ellipticity could switch from following that of the pump to an ellipticity of the opposite sign. It was recognized that this was a consequence of the existence of two steady-state solutions, termed here in-phase and out-of-phase, although the reason why the system chose one solution over the other was not found. Now, however, the stability analysis reveals that the sections of the in-phase and out-of-phase solutions that appear in a time-dependent solution are selected by the condition that the steady-state solutions are stable against small perturbations. The stability analysis was also applied to a second QD spin-VCSEL structure and was again able to account for the detailed polarization behavior found from time-dependent solutions. Thus, it has been shown that a stability analysis provides a useful tool in studying the polarization properties of QD spin-VCSELs, and hence future work will address the application of this technique to gain a clearer interpretation of the behavior observed in experimental studies of these devices.

Author Contributions: M.A. and D.A. conceived and developed the theory; N.L. and H.S. conceived and developed the stability analysis; N.L performed the numerical computations; M.A. and N.L. analyzed the data; I.H., H.S. and M.A. directed the research; M.A. wrote the paper.

References

1. Hallstein, S.; Berger, J.D.; Hilpert, M.; Schneider, H.C.; Rühle, W.W.; Jahnke, F.; Koch, S.W.; Gibbs, H.M.; Khitrova, G.; Oestreich, M. Manifestation of coherent spin precession in stimulated semiconductor emission dynamics. *Phys. Rev. B* **1997**, *56*, R7076–R7079. [CrossRef]
2. Ando, H.; Sogawa, T.; Gotoh, H. Photon-spin controlled lasing oscillation in surface-emitting lasers. *Appl. Phys. Lett.* **1997**, *73*, 566–568. [CrossRef]
3. Hendriks, R.F.M.; Van Exter, M.P.; Woerdman, J.P.; Gulden, K.H.; Moser, M. Memory effect for polarization of pump light in optically pumped vertical-cavity semiconductor lasers. *IEEE J. Quantum Electron.* **1998**, *34*, 1455–1460. [CrossRef]

4. Rudolph, J.; Hagele, D.; Gibbs, H.M.; Khitrova, G.; Oestreich, M. Laser threshold reduction in a spintronic device. *Appl. Phys. Lett.* **2003**, *82*, 4516–4518. [CrossRef]

5. Li, M.; Jähme, H.; Soldat, H.; Gerhardt, N.; Hofmann, M.; Ackemann, T. Birefringence controlled room-temperature picosecond spin dynamics close to the threshold of vertical-cavity surface-emitting laser devices. *Appl. Phys. Lett.* **2010**, *97*, 191114. [CrossRef]

6. Gerhardt, N.C.; Hofmann, M.R. Spin-controlled vertical-cavity surface-emitting lasers. *Adv. Opt. Technol.* **2012**, *2012*, 268949. [CrossRef]

7. Žutic, I.; Fabian, J.; Sarma, S.D. Spintronics: Fundamentals and applications. *Rev. Mod. Phys.* **2004**, *76*, 323–410. [CrossRef]

8. Bhattacharya, P.; Basu, D.; Das, A.; Saha, D. Quantum dot polarized light sources. *Semicond. Sci. Technol.* **2011**, *26*, 014002. [CrossRef]

9. Basu, D.; Saha, D.; Wu, C.C.; Holub, M.; Mi, Z.; Bhattacharya, P. Electrically injected InAs/GaAs quantum dot spin laser operating at 200 K. *Appl. Phys. Lett.* **2008**, *92*, 091119. [CrossRef]

10. Saha, D.; Basu, D.; Bhattacharya, P. High-frequency dynamics of spin-polarized carriers and photons in a laser. *Phys. Rev. B* **2010**, *82*, 205309. [CrossRef]

11. Alharthi, S.S.; Orchard, J.; Clarke, E.; Henning, I.D.; Adams, M.J. 1300 nm optically pumped quantum dot spin vertical external-cavity surface-emitting laser. *Appl. Phys. Lett.* **2015**, *107*, 151109. [CrossRef]

12. Oszwałdowski, R.; Gøthgen, C.; Žutić, I. Theory of quantum dot spin lasers. *Phys. Rev. B* **2010**, *82*, 085316. [CrossRef]

13. Lee, J.; Falls, W.; Oszwałdowski, R.; Žutić, I. Mapping between quantum dot and quantum well lasers: From conventional to spin lasers. *Phys. Rev. B* **2012**, *85*, 045314. [CrossRef]

14. Qasaimeh, O. Effect of doping on the polarization characteristics of spin-injected quantum dot VCSEL. *Opt. Quantum Electron.* **2015**, *47*, 465–476. [CrossRef]

15. Qasaimeh, O. Novel closed-form solution for spin-polarization in quantum dot VCSEL. *Opt. Commun.* **2015**, *350*, 83–89. [CrossRef]

16. Alexandropoulos, D.; Al-Seyab, R.K.; Henning, I.D.; Adams, M.J. Instabilities in quantum-dot spin-VCSELs. *Opt. Lett.* **2012**, *37*, 1700–1702. [CrossRef] [PubMed]

17. Adams, M.J.; Alexandropoulos, D. Analysis of quantum-dot spin-VCSELs. *IEEE Photon. J.* **2012**, *4*, 1124–1132. [CrossRef]

18. San Miguel, M.; Feng, Q.; Moloney, J.V. Light-polarization dynamics in vertical cavity surface-emitting lasers. *Phys. Rev. A* **1995**, *52*, 1728–1739. [CrossRef] [PubMed]

19. Gahl, A.; Balle, S.; San Miguel, M. Polarization dynamics of optically pumped VCSELs. *IEEE J. Quantum Electron.* **1999**, *35*, 342–351. [CrossRef]

20. Susanto, H.; Schires, K.; Adams, M.J.; Henning, I.D. Spin-flip model of spin-polarized vertical-cavity surface-emitting lasers: Asymptotic analysis, numerics, and experiments. *Phys. Rev. A* **2015**, *92*, 063838. [CrossRef]

21. Homoyanfour, A.; Adams, M.J. Analysis of SFM dynamics in solitary and optically-injected VCSELs. *Opt. Express* **2007**, *15*, 10504–10519. [CrossRef]